Robust Visible-Light Photocatalytic Norfloxacin Degradation from Aqueous Solution Using Ni-doped ZnO/ MWCNTs Nanocomposite

Shiwei Wen[1,], Mi Chen[2] and Hui Cao[3]*

[1] Zhongshanhaohui metal products co., ltd, Zhongshan 528400, China
[2] School of Management, University of Electronic Science and Technology of China, Zhongshan Institute, Zhongshan 528400, China
[3] Library, Zhongshan shaxi science & engineering school，Zhongshan 528400, China
[*]E-mail:wenshiwei2021@sina.com

This study revealed the preparation of Ni-doped ZnO/ MWCNTs nanocomposite as a photocatalyst for degradation of norfloxacin as quinolone under UV and visible light irradiations. The chemical synthesis method was used for functionalization of MWCNTs to prepare Ni-doped ZnO/MWCNTs nanocomposite. SEM and XRD analyses of the nanocomposite revealed that it was composed of Ni-doped ZnO spherical nanoparticles attached to a tangled network of MWCNTs. EIS and CV studies revealed that Ni-doped ZnO/MWCNTs composites had improved interfacial charge transfer efficiency. Optical studies revealed that the band gap energy for Ni-doped ZnO/MWCNTs nanocomposites was 2.90 eV, and anchoring Ni into the MWCNTs and ZnO lattices resulted in a narrowing of the nanocomposite band gap. The photocatalytic studies revealed that after 30, 60, 120, and 160 minutes of visible irradiation, respectively, and 40, 70, 150, and 200 minutes of UV irradiation, respectively, complete degradation of 10, 20, 50, and 100 mg/l of norfloxacin was obtained. Results indicated that the synergetic effect of functionalized MWCNTs and Ni NPs in anocomposite caused the band gap to narrow and could provide higher redox abilities under visible light irradiation and enhance the range of a sensitization process due to form facile electron transfer and the heterojunction formation.

1. INTRODUCTION

Quinolones as synthetic antibiotics are a broad class of antibacterial agents which contain a bicyclic ring structure of 4-quinolone. Quinolones interfere with DNA replication by blocking the resealing of the DNA double-strand break and preventing bacterial DNA from unwinding and duplicating. Fluoroquinolones (FQs) are the major clinical class of quinolones which differ from

quinolones through the addition of a fluorine atom at the sixth position in the central ring system. FQs act as strong antibiotics against both Gram-negative and Gram-positive bacteria. FQs antibiotics such as norfloxacin, enoxacin, pefloxacin, ofloxacin and ciprofloxacin are frequently used to treat genitourinary infections, pyelonephritis or bacterial prostatitis, sickle-cell disease, osteomyelitis and pneumonia [1-3].

However, FQs are usually well tolerated with few typical mild-to-moderate side effects that the susceptible groups of patients such as children and the elderly are at greater risk of adverse reactions during therapeutic use. Studies on FQs have shown the possibility of disabling and potentially permanent serious side effects. These side effects are the risk of damage to tendons, muscles, aorta joints, nerves, and central nervous system. The nerve damage causes mental health problems such as insomnia, restlessness, and rarely, seizures, convulsions, and psychosis [4-6].

The strong binding of FQs to soil/sediment causes the biodegradation process to be delayed. Thus, many observations have indicated the presence of FQs in the sludge of domestic wastewater treatment plants and pharmaceutical wastewater which could cause some problems in humans and animals due to genotoxic potential, physiological teratogenesis of plants/algae, antibiotic resistance and potential of photocarcinogenic properties. Therefore, many studies have been conducted on treatment of FQs from wastewater through electrochemical oxidation, Fenton oxidation, ozonation, chlorination, ion exchange filtration and photocatalysis [7-10]. Among these treatment methods, photocatalytic degradation of FQ on semiconductors such as TiO_2 and ZnO under UV or visible light irradiations is an interesting technique due to its low toxicity, low cost, environmentally friendly process and sustainable technology [11-13].

However, the practical application of photocatalytic degradation is limited because of the low light harvesting ability, backward reactions and poor absorption ability [14, 15]. Further studies have been revealed that the nanostructured heterogeneous photocatalysts could overcome these problems because of its high surface area and a high interfacial charge transfer rate [16-22]. Therefore, this study revealed the synthesis of Ni-doped ZnO/ MWCNTs NC and its application to photocatalytic degradation of norfloxacin (NOR) from aqueous solution.

2. MATERIALS and METHOD

MWCNTs, ZnO NPs, Ni-doped ZnO NPs, ZnO/ MWCNTs and Ni-doped ZnO/MWCNTs nanocomposites were synthesized on Si and glassy carbon electrode as substrates. In order to preparation of ZnO/MWCNTs and Ni-doped ZnO/MWCNTs nanocomposites, 5g MWCNTs (97.5%, Chengdu Bravecount Trading Co., Ltd., China) was ultrasonically functionalized in concentrated H_2SO_4 (98%, Sigma-Aldrich) and HNO_3 (70%, Sigma-Aldrich) with a volume ratio of 3:1 at 50°C for 6 hours. The functionalized MWCNTs were filtered and washed several times with deionized water and acetone, respectively. The suspension was then dried in a vacuum oven at 75°C for 12 hours. At 70 °C for 12 hours, 2 g of the final product was ultrasonically distributed in 20 ml dimethyl formamide (DMF, 99.8%, Sigma-Aldrich). The dispersed MWCNTs were then treated with 6 ml of 0.1 M zinc acetate solution (99%, Haihang Industry Co., Ltd., China) and 1 ml of 1 mM nickel nitrate hexahydrate

(99%, W&Q Metal Products Co., Limited, China). After 30 minutes of magnetic stirring at 35°C, the sample was centrifuged at 1000 rpm for 5 minutes, washed with deionized water several times, and then dried in an oven at 80°C for 5 hours. The substance was calcined in vacuum for 10 hours at 280°C.

The morphology and crystal structure of nanocomposite were studied using scanning electron microscopy (SEM, Hitachi S-4700II, Tokyo, Japan) and X-ray diffraction (XRD, Bruker-AXS, Billerica, MA, USA) respectively. Optical studies were conducted on record of UV-visible absorption spectra of nanocomposite using an optical spectrophotometer (Hitachi Model U-3010). Electrochemical impedance spectroscopy (EIS) and cyclic voltammetry (CV) studies were conducted on Metrohm Autolab potentiostat (PGSTAT204, Metrohm Autolab, Netherlands) in a three-electrode electrochemical cell containing Ag/AgCl, Pt wire and modified nanocomposited/glassy carbon electrode as reference, counter and working electrodes, respectively. The electrochemical measurement was performed in 0.1M phosphate buffer solutions (PBS) aqueous solutions (pH 6.8) containing 5 mM [Fe $(CN)6]^{4-/3-}$ (≥99.0%, Sigma-Aldrich). 0.1 M PBS was prepared using 0.1 M NaH_2PO_4 (≥98%, Sigma-Aldrich) and 0.1 M Na_2HPO_4 (≥99.0%, Sigma-Aldrich) in a volume ratio of 1:1.

The photocatalytic studies were carried out for degradation of NOR (>99%, SCM Pioneering Co., Ltd., China) using prepared nanocomposite as photocatalysts. Prior to the degradation measurements, the NOR solution and photocatalyst were held in the dark for 30 minutes to reach the balance of adsorption-desorption. The concentration of the solution was determined using a UV–vis spectrophotometer as following equation [20]:

$$\text{Degradation efficiency} = \frac{I_0 - I}{I_0} \times 100 = \frac{C_0 - C}{C_0} \times 100 \qquad (1)$$

Where I_0 is the initial absorbance peak density, I is the absorbance peak density after light irradiation, and C_0 and C are the initial concentration and concentration of NOR solution after light irradiation, respectively.

3. RESULTS AND DISCUSSION

SEM images in Figure 1 show the surface morphology of Ni-doped ZnO NPs and Ni-doped ZnO/ MWCNTs nanocomposites. As observed from Figure 1a, Ni-doped ZnO NPs had a spherical shape with an average diameter of 90 nm. The morphology of the Ni-doped ZnO/MWCNTs nanocomposite shows that the Ni-doped ZnO NPs are uniformly distributed on the surface of the MWCNTs and that there is less agglomeration of nanoparticles on the MWCNTs surface, indicating a strong interphase structure effect between the Ni-doped ZnO NPs and the MWCNTs. Moreover, increasing surface area of the Ni-doped ZnO/MWCNTs nanocomposite can enhance the photocatalytic performance [23].
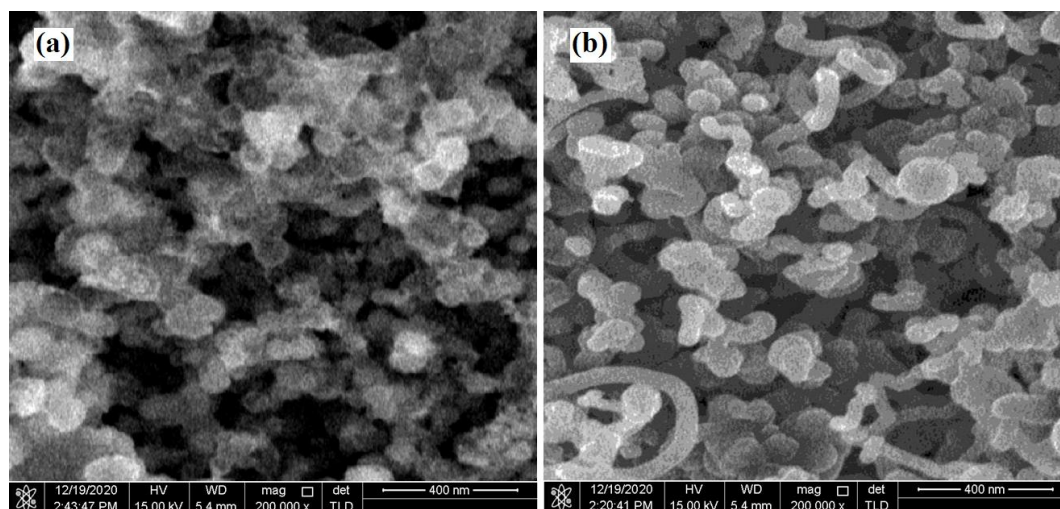
Figure 1. FESEM image of (a) Ni-doped ZnO NPs, (b) Ni-doped ZnO/MWCNTs nanocomposites
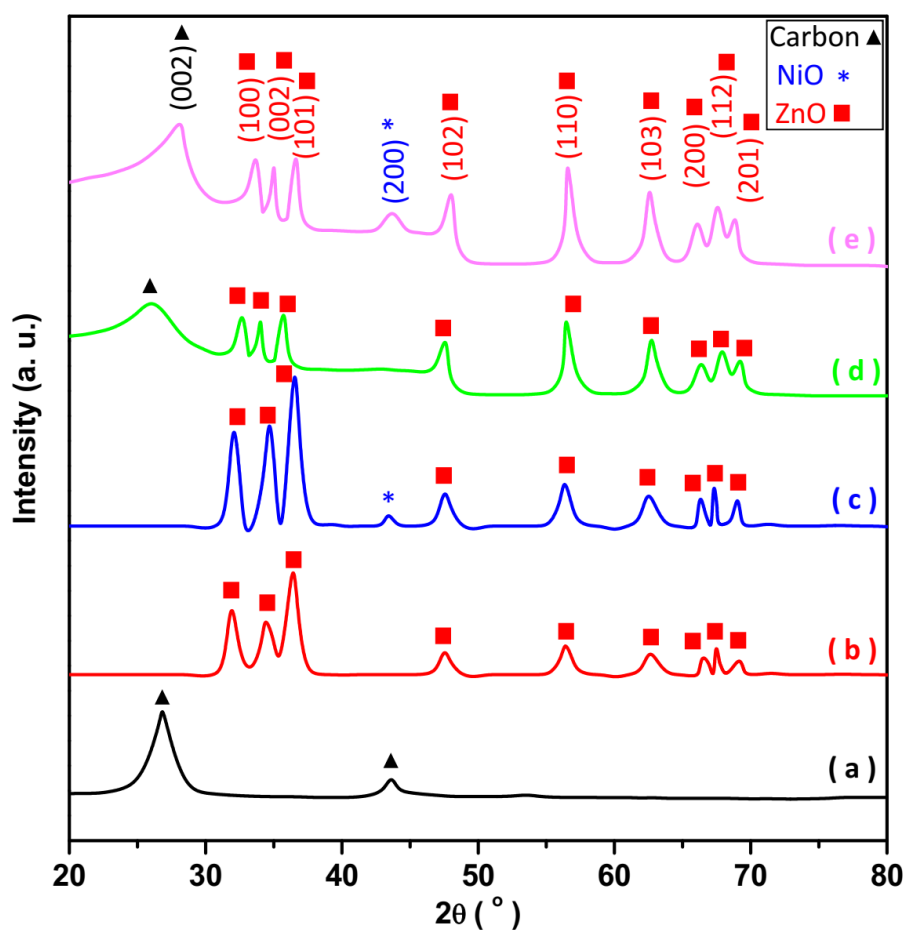

Figure 2. XRD pattern of (a) MWCNTs, (b) ZnO NPs, (c) Ni-doped ZnO NPs, (d) ZnO/MWCNTs and (e) Ni-doped ZnO/MWCNTs nanocomposite
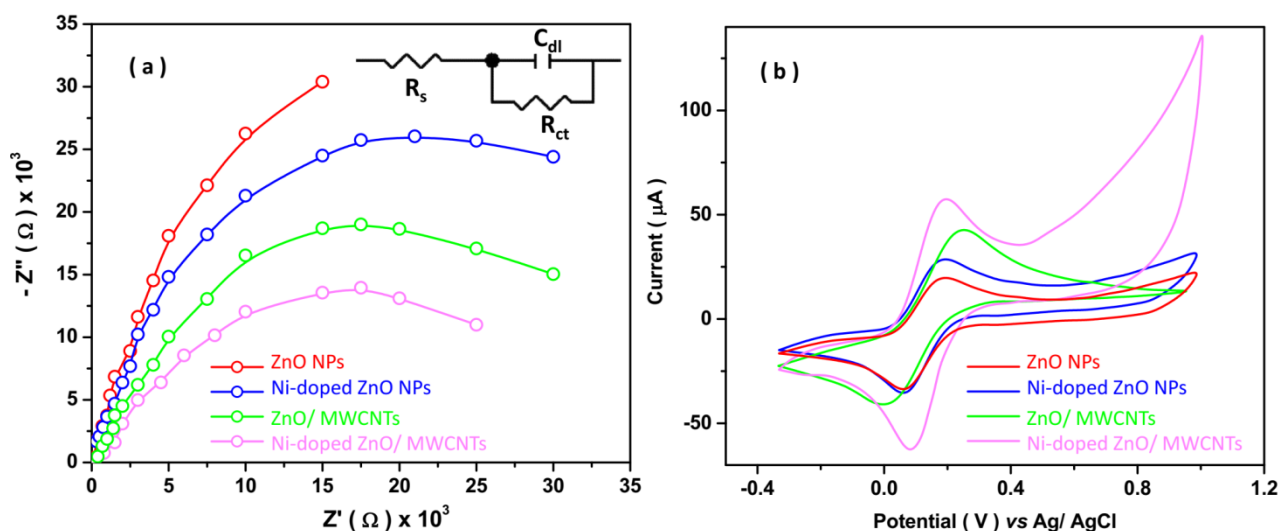
Figure 3. (a) Nyquist plots in the frequency range of 10^{-1} Hz to 10^5 Hz at AC voltage amplitude of 5 mV, and (b) CV curves of ZnO NPs, Ni-doped ZnO NPs, ZnO/MWCNTs and Ni-doped ZnO/MWCNTs nanocomposites on modified glassy carbon electrode 0.1M PBS (pH 6.8) containing 5 mM [Fe (CN)6]$^{4-/3-}$ in sacn rate of 100 mV/s.

The XRD patterns of MWCNTs, ZnO NPs, Ni-doped ZnO NPs, ZnO/MWCNTs and Ni-doped ZnO/MWCNTs nanocomposite are represented in Figure 2. The diffraction pattern of MWCNTs, as seen in Figure 2a, shows two diffraction peaks at 26.75° and 43.61°, which are indexed to the formation of (002) and (100) planes of hexagonal graphitic structure of MWCNTs, respectively, and are well-matched with the JCPDS card No.41-1487. Figure 2b shows ZnO NPs with diffraction peaks at 31.88°, 34.37°, 36.51°, 47.63°, 56.38°, 62.66°, 66.49°, 67.61°, and 69.38°, which correspond to the (100), (002), (101), (102), (110), (103), (200), (112), and (201) planes of the wurtzite structure of ZnO. The XRD patterns of Ni-doped ZnO NPs in Figure 2c show an additional diffraction peak at 43.39° that is indexed to the (200) plane of NiO, which can be attributed to the Ni substitution into the ZnO lattice [24]. The XRD pattern of ZnO/MWCNTs in Figure 2d displays the all diffraction peaks of ZnO and (002) plane of MWCNTs. In comparison to other XRD patterns, the XRD pattern of Ni-doped ZnO/MWCNTs in Figure 2e shows all diffraction peaks of ZnO, (200) plane of NiO and (002) plane of MWCNTs that indicated the introduction of Ni into ZnO/MWCNTs nanocomposite [24].

Electrochemical studies of ZnO NPs, Ni-doped ZnO NPs, MWCNTs/ZnO and Ni-doped ZnO/MWCNTs nanocomposites were conducted on EIS and CV measurements in 0.1M PBS (pH 6.8) containing 5 mM [Fe (CN)6]$^{4-/3-}$ as electrolyte under visible light illumination. Figure 3a shows the nyquist plots of prepared electrodes and the related equivalent circuit. The charge transfer resistance (Rct) is determined by the semicircle diameter and can be related to electron transfer reactions such as rate of rate kinetics kinetics [25]. The smaller semicircle diameter of ZnO NPs and Ni-doped ZnO NPs indicates the considerable enhanced interfacial charge transfer efficiency that signifies the improvement of photoinduced charge carrier separation in ZnO/MWCNTs and Ni-doped ZnO/MWCNTs composites. The lowest Rct of Ni-doped ZnO/MWCNTs composite reveals the synergistic effect of MWCNTs and Ni NPs over the surface of ZnO NPs. MWCNTs can act as a

charge transfer channel for accelerating electron transfer between Ni and ZnO NPs and effectively decrease the recombination of electron-hole pairs in Ni-doped ZnO/MWCNTs composite [26-28]. Moreover, the CV curves in Figure 3b show the redox peak current is remarkably increased when the glassy carbon electrode surface is modified with Ni-doped ZnO/MWCNTs composite because of its great electron transfer ability. As observed, this modification can increase the effective surface area and the number of active sites and defects in composite and enhance rapid and efficient transfer of photogenerated carriers [29-31].
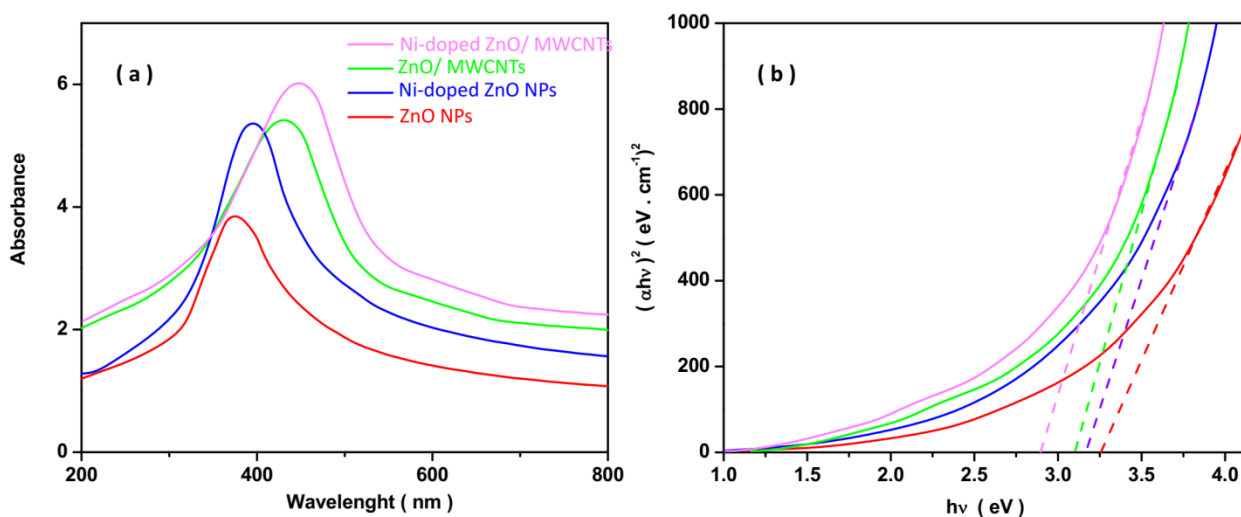

Figure 4. (a) UV–vis absorption spectra and (a) Tauc curves of ZnO NPs, Ni-doped ZnO NPs, ZnO/MWCNTs and Ni-doped ZnO/MWCNTs nanocomposites.

Figure 4a exhibits the UV–vis absorption spectrum of ZnO NPs, Ni-doped ZnO NPs, ZnO/MWCNTs and Ni-doped ZnO/MWCNTs nanocomposites. The absorption edges are observed at 375, 391, 429 and 448 nm for ZnO NPs, Ni-doped ZnO NPs, ZnO/MWCNTs and Ni-doped ZnO/MWCNTs nanocomposites, respectively. Therefore, the band absorption edges are red shifted. The maximum absorption and red shift of absorption edge of Ni-doped ZnO/MWCNTs nanocomposite obviously demonstrate that Ni^{2+} ions are incorporated into the ZnO lattice [32]. The Tauc equation was used for determination of the band-gap energy (Eg) as following equation [33, 34]:

$$(\alpha h\nu)^2 = A(h\nu - Eg) \qquad (2)$$

Where α and $h\nu$ refer to absorption coefficient and the photonenergy. Eg can be calculated from the intercept of a straight line on the $h\nu$ axis in a plot of $(\alpha h\nu)^2$ versus $h\nu$[33, 34]. Figure 4b shows that the Eg are obtained 3.25, 3.17, 3.11, 2.90 eV for ZnO NPs, Ni-doped ZnO NPs, ZnO/MWCNTs and Ni-doped ZnO/MWCNTs nanocomposites, respectively which indicated to anchoring Ni into the MWCNTs and ZnO lattice leads to Ni-doped ZnO/MWCNTs nanocomposite Eg narrower in compare with ZnO NPs and ZnO/MWCNTs nanocomposites. By the introduction of the Ni particles, the Fermi

level enters the conduction band in different degrees and the sp–d Exchange interactions between the band electrons and the localized d-electrons of the Ni^{2+} ions are changed [35]. The conduction band moves down and the band gap is decreased toward the ZnO NPs, ZnO/MWCNTs nanocomposite because of creation impurity energy levels of 3d contribution of Ni atoms [36]. These impurity energy levels also act as a spring board for electrons to transition from valence band to conduction band, thereby decreasing the required energy for electron transition [35, 36].
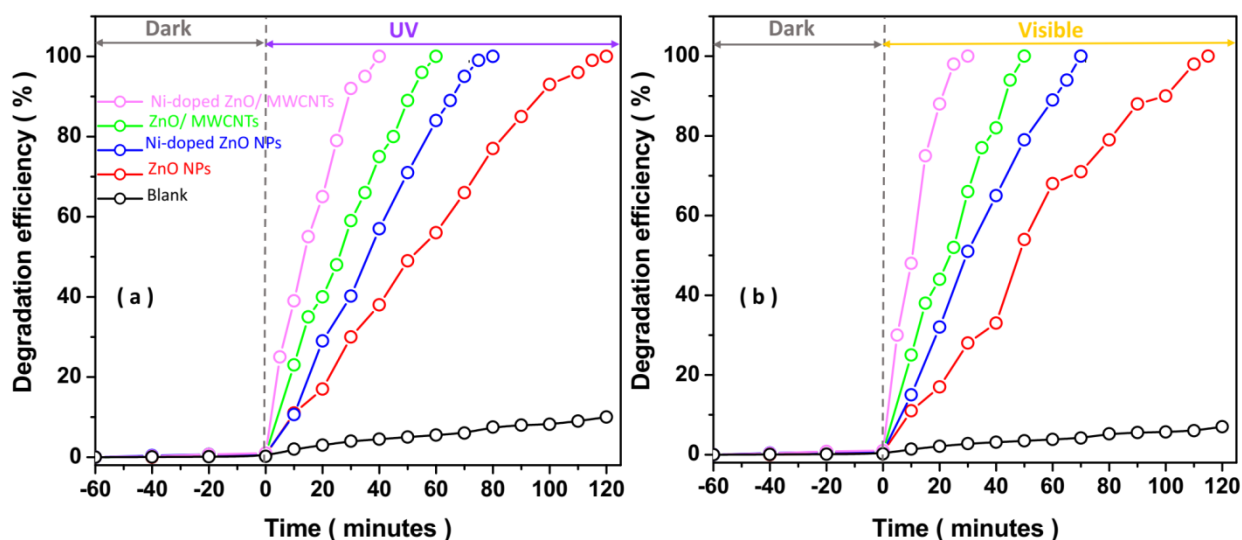

Figure 5. Degradation efficiencies of 10mg/l NOR (pH 6.8) on ZnO NPs, Ni-doped ZnONPs, ZnO/ MWCNTs and Ni-doped ZnO/ MWCNTsnanocomposites under (b) UV and (a) visible light irradiation.

The photdegradation efficiency of 10mg/l NOR, in the bulk solution (without the photocatalyst), and the existence of ZnO NPs, Ni-doped ZnO NPs, ZnO/MWCNTs and Ni-doped ZnO/MWCNTs nanocomposites as photocatalysts in dark and under irradiation UV is displayed in Figure 5a. As seen, there isn't any insignificant degradation of NOR (less than 1%) for all samples in the first 60 minutes in the dark, which implies light's effective role in degradation reactions. For the second 120 minutes, it can be observed that the blank experiments show less than 10% degradation under UV irradiation. Furthermore, the NOR concentration is decreased over time in the presence of the photocatalysts. Photocatalytic performance of samples reveals over 40 minutes of UV irradiation, Ni-doped ZnO/MWCNTs causes the complete removal of 10 mg/l NOR, which indicated its significant degradation activity compared to ZnO NPs and ZnO/MWCNTs nanocomposite.

The photocatalytic degradation measurements of 10 mg/l NOR were also evaluated under visible light irradiation. Figure 5b exhibits that the 100% degradation efficiency of ZnO NPs, Ni-doped ZnO NPs, ZnO/MWCNTs and Ni-doped ZnO/MWCNTs nanocomposites are obtained after 115, 70, 50 and 30 minutes of visible light irradiation, respectively. Therefore, the higher efficiency is achieved for Ni-doped ZnO/MWCNTs under both UV and visible light irradiation. It can be related to change of photosensitization and catalytic properties of nanocomposite in the presence of MWCNTs and Ni

particles. MWCNTs show high specific surface area and electron transition rate that can provide more binding sites for substrate molecules to adsorb pollutant molecules, leading to enhanced photodegradation rate [37]. In addition, MWCNTs as nanostructured carbonaceous materials exhibit the considerable electron storage capacity (one electron for every 32 carbon atoms) that MWCNTs can act as the electron sink and accept photogenerated electrons [38]. Moreover, the observed enhancement of photodegradation rate in ZnO/MWCNTs toward ZnO NPs, Ni-doped ZnO NPs can be related to the type of bonds and interactionsof MWCNTs in the structure, which could enhance the absorbance of visible light [39]. As a consequence, it decreases the recombination of photogenerated electrons and holes through formation the trapping channels for electrons [40]. Simultaneously, photo-induced holes in the valance band can react with NOR molecules, aiding in the degradation process [41]. According to the optical results, the introduction of MWCNTs and Ni narrows the band gap energy of ZnO NPs. The red shift of absorption edge indicates the extend of absorption in the visible-light region [42]. Narrowing the Ni-doped ZnO/MWCNTs band gap like a heterojunction photocatalytic systems can provide higher redox abilities. In the most common mechanism, a narrow band gap of the resulting heterostructure of combination MWCNTs and metal oxide doped into ZnO enhances the ranges of the sensitization process due to easy electron transfer and heterojunction formation [43]. The photogenerated carriers can migrate from a semiconductor material with a higher conduction band to another with an inferior conduction band which can promote the photocatalytic efficiencies of wide bandgap semiconductors such as ZnO for visible light harvesting [43].In addition, doping the Ni can efficiently reduce the recombination chance of excitions and the photoinduced electrons and holes could be trapped around the dopant because of inducing the distortion of local electric field [44].Therefore, further photocatalytic studies were performed using Ni-doped ZnO/MWCNTs.

Figure 6 shows the effect of different initial NOR concentrations on the photodegradation efficiency of Ni-doped ZnO/MWCNTs under UV and visible irradiations. It is observed that the degradation efficiency decreases remarkably with the increase of the initial concentration of NOR. The complete degradation of 10, 20, 50 and 100 mg/l of NOR is obtained after 30, 60, 120 and 160 min of visible irradiation, respectively, and after 40, 70, 150 and 200 minutes of UV radiation, respectively. The lowest degradation efficiency is obtained at 100 mg/l initial concentration of NOR that could be associated with occupation of photoactive sites on Ni-doped ZnO/MWCNTs surface in presence of the excessive NOR molecules in the solution. Moreover, the path length of the entering photons can be decreased due to scattering of the excessive NOR molecules in the solution. Thus, a decrease in photoactive sites could decrease the formation of hydroxyl radicals.
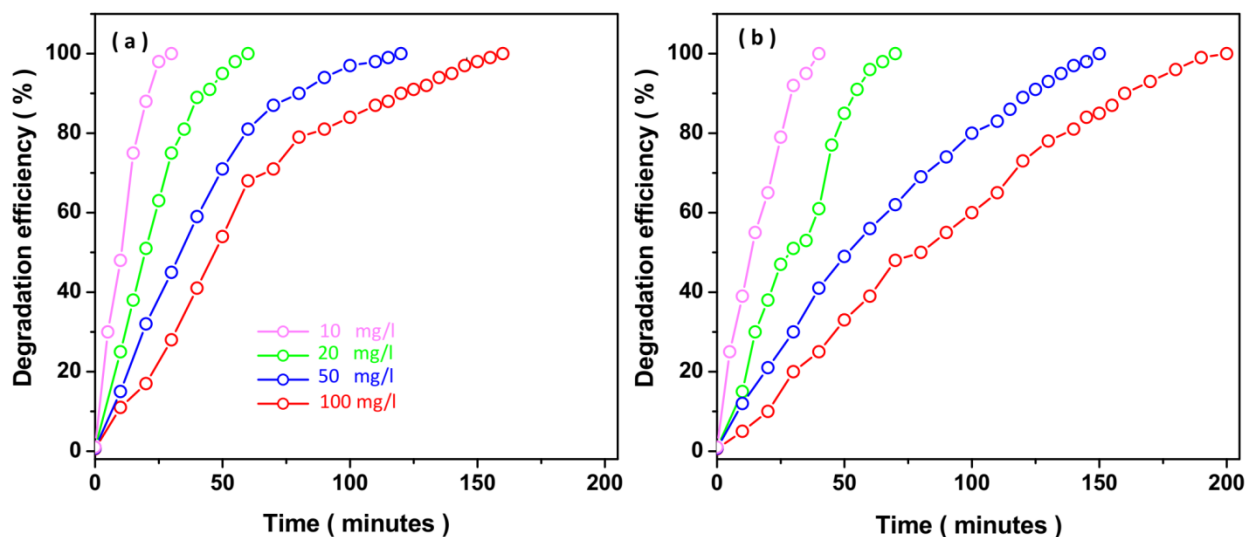
Figure 6. Effect of initial NOR content on the degradation efficiencies of Ni-doped ZnO/MWCNTs under (a) visible light and (b) UV irradiations (pH 6.8)

Table 1 represents an evaluation between the degradation efficiencies of Ni-doped ZnO/MWCNTs nanocomposite and the other reported photocatalysts for degradation of NOR. It is found that the prepared nanocomposite in this study shows a higher degradation rate of 50 and 100 mg/l NOR. It can be concluded that the Ni-doped ZnO/MWCNTs nanocomposite could be an effective photocatalyst for degradation of high concentration of NOR.

Table 1. Evaluation between the degradation efficiencies of Ni-doped ZnO/MWCNTs nanocomposite and other reported photocatalysts for degradation of NOR.

Catalyst	NOR initial concentration(mg/l)	Light source	Irradiation time(min)	Degradation efficiency (%)	Ref.
Co_3O_4/Bi_2MoO_6	-	Visible	30	87.68	[45]
N-doped TiO_2	6.03	Visible	30	99.53	[11]
BiFe-ZnO	10	Solar light	120	80	[12]
Ag@$BiPO_4$/BiOBr/$BiFeO_3$	20	UV Visible	45 90	99.1 98.1	[8]
$CoTiO_3$/UiO-66-NH_2	20	Solar light	60	90.13	[46]
Triton-X100/Bi_2WO_6	20.11	Visible	120	100	[47]
$ZnFe_2O_4$-carbon allotropes	50	Solar light	90	91.36	[9]
Ag NPs	75	Visible	100	100.0	[7]
Ni-doped ZnO/MWCNTs	10	UV Visible	40 30	100.0 100.0	This work
Ni-doped ZnO/MWCNTs	20	UV Visible	70 60	100.0 100.0	This work
Ni-doped ZnO/MWCNTs	50	UV Visible	150 120	100.0 100.0	This work
Ni-doped ZnO/MWCNTs	100	UV Visible	200 160	100.0 100.0	This work

4. CONCLUSION

The present work was focused on preparation of Ni-doped ZnO/MWCNTs nanocomposite and application as a photocatalyst for degradation of NOR under UV and visible light irradiation. The Ni-doped ZnO/MWCNTs nanocomposite was synthesized using a chemical method with functionalized MWCNTs. The structural studies of the nanocomposite revealed that it was made up of Ni-doped ZnO spherical nanoparticles that were anchored on a tangled network of MWCNTs. Electrochemical studies revealed that Ni-doped ZnO/MWCNTs composites have improved interfacial charge transfer efficiency. The band gap energy for ZnO NPs, Ni-doped ZnO NPs, ZnO/MWCNTs, and Ni-doped ZnO/MWCNTs nanocomposites was 3.25, 3.17, 3.11, and 2.90 eV, respectively, indicating that anchoring Ni into the MWCNTs and ZnO lattice led to a narrowing of the nanocomposite band gap. According to the photocatalytic studies, complete degradation of 10, 20, 50, and 100 mg/l norfloxacin was obtained after 30, 60, 120, and 160 minutes of visible irradiation, and after 40, 70, 150, and 200 minutes of UV irradiation, respectively. The results demonstrated that narrowing the Ni-doped ZnO/MWCNTs band gap can provide higher redox abilities under visible light irradiation and increase the range of a sensitization process due to easy electron transfer and heterojunction formation.

References

1. K. Drlica and M. Malik, *Current topics in medicinal chemistry*, 3 (2003) 249.
2. R.C. Owens Jr and P.G. Ambrose, *Clinical infectious diseases*, 41 (2005) S144.
3. J. Rouhi, S. Kakooei, M.C. Ismail, R. Karimzadeh and M.R. Mahmood, *International Journal of Electrochemical Science*, 12 (2017) 9933.
4. C. Carbon, *Chemotherapy*, 47 (2001) 9.
5. L. Mandell and G. Tillotson, *Canadian Journal of Infectious Diseases*, 13 (2002) 54.
6. H. Karimi-Maleh, Y. Orooji, A. Ayati, S. Qanbari, B. Tanhaei, F. Karimi, M. Alizadeh, J. Rouhi, L. Fu and M. Sillanpää, *Journal of Molecular Liquids*, 329 (2021) 115062.
7. K. Kanagamani, P. Muthukrishnan, K. Shankar, A. Kathiresan, H. Barabadi and M. Saravanan, *Journal of Cluster Science*, 30 (2019) 1415.
8. A. Kumar, S.K. Sharma, G. Sharma, A.a.H. Al-Muhtaseb, M. Naushad, A.A. Ghfar and F.J. Stadler, *Journal of Hazardous Materials*, 364 (2019) 429.
9. A. Behera, S. Mansingh, K.K. Das and K. Parida, *Journal of Colloid and Interface Science*, 544 (2019) 96.
10. H. Karimi-Maleh, Y. Orooji, F. Karimi, M. Alizadeh, M. Baghayeri, J. Rouhi, S. Tajik, H. Beitollahi, S. Agarwal and V.K. Gupta, *Biosensors and Bioelectronics*, 184 (2021) 113252.
11. X. Jin, X. Zhou, P. Sun, S. Lin, W. Cao, Z. Li and W. Liu, *Chemosphere*, 237 (2019) 124433.
12. N.S. Shah, J.A. Khan, M. Sayed, Z.U.H. Khan, A.D. Rizwan, N. Muhammad, G. Boczkaj, B. Murtaza, M. Imran, H.M. Khan and G. Zaman, *Chemical Engineering Journal*, 351 (2018) 841.
13. H. Karimi-Maleh, M.L. Yola, N. Atar, Y. Orooji, F. Karimi, P.S. Kumar, J. Rouhi and M. Baghayeri, *Journal of colloid and interface science*, 592 (2021) 174.
14. P. Chen, H. Liu, W. Cui, S.C. Lee, L.a. Wang and F. Dong, *EcoMat*, 2 (2020) e12047.
15. C. Liu and J. Rouhi, *RSC Advances*, 11 (2021) 9933.
16. R. Hassanzadeh, A. Siabi-Garjan, H. Savaloni and R. Savari, *Materials Research Express*, 6 (2019) 106429.

17. J.C. Colmenares, R. Luque, J.M. Campelo, F. Colmenares, Z. Karpiński and A.A. Romero, *Materials*, 2 (2009) 2228.
18. H. Karimi-Maleh, M. Alizadeh, Y. Orooji, F. Karimi, M. Baghayeri, J. Rouhi, S. Tajik, H. Beitollahi, S. Agarwal and V.K. Gupta, *Industrial & Engineering Chemistry Research*, 60 (2021) 816.
19. Y. Yu, *International Journal of Electrochemical Science*, 16 (2021) 210259.
20. B. Gong, P. Wu, J. Yang, X. Peng, H. Deng and G. Yin, *International Journal of Electrochemical Science*, 16 (2021) 21023.
21. H. Savaloni, E. Khani, R. Savari, F. Chahshouri and F. Placido, *Applied Physics A*, 127 (2021) 1.
22. H. Karimi-Maleh, S. Ranjbari, B. Tanhaei, A. Ayati, Y. Orooji, M. Alizadeh, F. Karimi, S. Salmanpour, J. Rouhi and M. Sillanpää, *Environmental Research*, 195 (2021) 110809.
23. B.A. El-Sayed, W.A.A. Mohamed, H.R. Galal, H.M. Abd El-Bary and M.A.M. Ahmed, *Egyptian Journal of Petroleum*, 28 (2019) 247.
24. P. Shukla and J.K. Shukla, *Physica B: Condensed Matter*, 569 (2019) 31.
25. A.R. Bredar, A.L. Chown, A.R. Burton and B.H. Farnum, *ACS Applied Energy Materials*, 3 (2020) 66.
26. Z. Savari, S. Soltanian, A. Noorbakhsh and A. Salimi, *Electrochemical Society Iran*, 9 (2013) 1.
27. J. Ke, F. He, H. Wu, S. Lyu, J. Liu, B. Yang, Z. Li, Q. Zhang, J. Chen, L. Lei, Y. Hou and K. Ostrikov, *Nano-Micro Letters*, 13 (2020) 24.
28. I. Ahmad, M.S. Akhtar, E. Ahmed, M. Ahmad and M.Y. Naz, *Journal of Colloid and Interface Science*, 584 (2021) 182.
29. X. Li, J. Xiong, Y. Xu, Z. Feng and J. Huang, *Chinese Journal of Catalysis*, 40 (2019)
30. M. Srivastava, N.R. Nirala, S. Srivastava and R. Prakash, *Scientific reports*, 8 (2018) 1.
31. Z. Savari, S. Soltanian, A. Noorbakhsh, A. Salimi, M. Najafi and P. Servati, *Sensors and Actuators B: Chemical*, 176 (2013) 335.
32. S. Deka and P.A. Joy, *Chemistry of materials*, 17 (2005) 6507.
33. M. Wang, S. Yuan, B. Lv and H. Yang, *International Journal of Electrochemical Science*, 16 (2021) 210248.
34. J. Zhu and Z. Jiang, *International Journal of Electrochemical Science*, 16 (2021) 210318.
35. K.J. Kim and Y.R. Park, *Applied Physics Letters*, 81 (2002) 1420.
36. Z. Ma, F. Ren, Y. Deng and A.A. Volinsky, *Optik*, 219 (2020)
37. B.A. El-Sayed, W.A. Mohamed, H.R. Galal, H. Abd El-Bary and M.A. Ahmed, *Egyptian Journal of Petroleum*, 28 (2019) 247.
38. A. Kongkanand and P.V. Kamat, *ACS nano*, 1 (2007) 13.
39. X. Rong, F. Qiu, C. Zhang, L. Fu, Y. Wang and D. Yang, *Ceramics International*, 41 (2015) 2502.
40. F. Hosseini, A. Kasaeian, F. Pourfayaz, M. Sheikhpour and D. Wen, *Materials Science in Semiconductor Processing*, 83 (2018) 175.
41. S. Sharma, A.O. Ibhadon, M.G. Francesconi, S.K. Mehta, S. Elumalai, S.K. Kansal, A. Umar and S. Baskoutas, *Nanomaterials*, 10 (2020) 910.
42. X. Chen, Z. Wu, Z. Gao and B.-C. Ye, *Nanomaterials*, 7 (2017) 258.
43. M.A. Johar, R.A. Afzal, A.A. Alazba and U. Manzoor, *Advances in Materials Science and Engineering*, 2015 (2015) 1.
44. J. Zhao, L. Wang, X. Yan, Y. Yang, Y. Lei, J. Zhou, Y. Huang, Y. Gu and Y. Zhang, *Materials Research Bulletin*, 46 (2011) 1207.
45. J. Guo, C.-H. Shen, J. Sun, X.-J. Xu, X.-Y. Li, Z.-H. Fei, Z.-T. Liu and X.-J. Wen, *Separation and Purification Technology*, 259 (2021) 118109.

46.   S. Subudhi, L. Paramanik, S. Sultana, S. Mansingh, P. Mohapatra and K. Parida, *Journal of Colloid and Interface Science*, 568 (2020) 89.
47.   L. Tang, J. Wang, G. Zeng, Y. Liu, Y. Deng, Y. Zhou, J. Tang, J. Wang and Z. Guo, *Journal of Hazardous materials*, 306 (2016) 295.